

# Phase field modeling of electrochemistry I: Equilibrium

J. E. Guyer,\* W. J. Boettinger,<sup>†</sup> and J. A. Warren<sup>‡</sup>

*Metallurgy Division, Materials Science and Engineering Laboratory,  
National Institute of Standards and Technology, Gaithersburg, MD 20899*

G. B. McFadden<sup>§</sup>

*Mathematical and Computational Sciences Division, Information Technology Laboratory,  
National Institute of Standards and Technology, Gaithersburg, MD 20899*

(Dated: February 7, 2020)

A diffuse interface (phase field) model for an electrochemical system is developed. We describe the minimal set of components needed to model an electrochemical interface and present a variational derivation of the governing equations. With a simple set of assumptions: mass and volume constraints, Poisson's equation, ideal solution thermodynamics in the bulk, and a simple description of the competing energies in the interface, the model captures the charge separation associated with the equilibrium double layer at the electrochemical interface. The decay of the electrostatic potential in the electrolyte agrees with the classical Gouy-Chapman and Debye-Hückel theories. We calculate the surface energy, surface charge, and differential capacitance as functions of potential and find qualitative agreement between the model and existing theories and experiments. In particular, the differential capacitance curves exhibit complex shapes with multiple extrema, as exhibited in many electrochemical systems.

PACS numbers: 73.30.+y, 81.15.Aa, 82.45.Mp, 82.45.Jn

## I. INTRODUCTION

We develop a phase field model of an electrochemical system. The method employs a phase field variable, which is a function of position and time, to describe whether the material is one phase or another (*i.e.*, the electrode or electrolyte). The behavior of this variable is governed by a partial differential equation (PDE) that is coupled to the relevant transport equations for the material. The interface between the phases is described by smooth but highly localized changes of this variable. This approach avoids the mathematically difficult problem of applying boundary conditions at an interface whose location is part of the unknown solution. The phase field method is powerful because it easily treats complex interface shapes and topology changes. One long range goal of the approach is to treat the complex geometry, including void formation, that occurs during plating in vias and trenches for on-chip metallization [1].

The phase field method has been used widely for solidification [2, 3]. The present approach is motivated by the mathematical analogy between the governing equations of solidification dynamics and electroplating dynamics. For example, the solid-melt interface is analogous to the electrode-electrolyte interface. The various overpotentials of electrochemistry have analogies with the supercoolings of alloy solidification: diffusional (constitutional), curvature and interface attachment. Dendrites

can form during solidification and during electroplating. It is not surprising, however, that we find significant differences between the two systems. The crucial presence of charged species in electrochemistry leads to rich interactions between concentration, electrostatic potential, and phase stability.

We first pick a minimal set of components required to describe the possible composition variations from the electrode to the electrolyte through the electrochemical interface. Next we define concentration and mole fraction variables. Then a variational principle is used to establish a set of PDE's that govern equilibrium interfaces. In a second paper [4], we explore dynamic solutions to the phase field equations.

Given a minimal set of assumptions, the model predicts the charge separation associated with the equilibrium double layer at the electrochemical interface. Changes in surface potential induce changes in surface energy (electrocapillary curves), surface charge, and differential capacitance. The decay length of charge in the electrolyte as a function of electrolyte concentration is consistent with the Debye-Hückel theory. The parameters of the phase field model are related to the physical parameters of traditional electrochemistry. The results are compared to the classic Gouy-Chapman-Stern model of the electrified interface [5, 6, 7, 8] as well as to experimental capacitance curves [9, 10].

\*Electronic address: [guyer@nist.gov](mailto:guyer@nist.gov)

<sup>†</sup>Electronic address: [william.boettinger@nist.gov](mailto:william.boettinger@nist.gov)

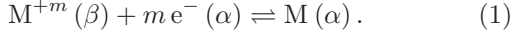
<sup>‡</sup>Electronic address: [jwarren@nist.gov](mailto:jwarren@nist.gov)

<sup>§</sup>Electronic address: [mcfadden@nist.gov](mailto:mcfadden@nist.gov)

## II. MODEL FORMULATION

### A. Choice of Components, Phases, and Molar Volumes

To treat an electrochemical system, we consider a set of components consisting of cations, anions, and electrons. We will refer to the metallic conducting electrode phase as  $\alpha$  and the ionic conducting electrolyte phase as  $\beta$ . In this diffuse interface model, the concentrations of the components will vary smoothly through the interfacial region. The electrode will be considered primarily a solution of two components: electrons  $e^-$  (component #1) and cations  $M^{+m}$  (component #2). The electrolyte will be considered primarily a solution of three components; more noble cations  $M^{+m}$  (component #2), less noble cations  $N^{+n}$  (component #3), and anions  $A^{-a}$  (component #4). The primary charge transfer reaction for this system is



For the solution behavior, all ions are treated as substitutional species with identical partial molar volumes  $\bar{V}_s$ . Electrons are treated as an interstitial species with zero partial molar volume. The interstitial nature is necessary to recover ohmic behavior in the electrode phase. We employ mole fractions  $X_j$  of each component  $j$  that have the conventional definition, such that

$$\sum_{j=1}^n X_j = 1, \quad (2)$$

where  $n = 4$  for the four-component system we consider in this paper. The molar volume varies because the mole fractions of the components vary from one phase, through the interface, and into the other phase. At each point it is given by

$$V_m = \sum_{j=1}^n \bar{V}_j X_j = \bar{V}_s \sum_{j=2}^n X_j, \quad (3)$$

where  $\bar{V}_j$  is the partial molar volume of each component  $j$ ,  $\sum_{j=1}^n$  is the sum over all components, and  $\sum_{j=2}^n$  is the sum over all substitutional components. The mole per volume concentrations are defined as  $C_j \equiv X_j/V_m$ , such that

$$\sum_{j=1}^n \bar{V}_j C_j = \bar{V}_s \sum_{j=2}^n C_j = 1. \quad (4)$$

Picking one component  $j = n$  with  $\bar{V}_n = \bar{V}_s \neq 0$ , we can always express its concentration in terms of the others as  $C_n = 1/\bar{V}_s - \sum_{j=2}^{n-1} C_j$ .

### B. Equilibrium

We propose a Helmholtz free energy for an isothermal system of charged components

$$F(\xi, C_1 \dots C_n, \phi) = \int_V \left( f_V(\xi, C_1 \dots C_n) + \frac{\kappa_\xi}{2} |\nabla \xi|^2 + \frac{1}{2} \rho \phi \right) dV \quad (5)$$

integrated over the volume  $V$ , where  $f_V$  is the Helmholtz free energy per unit volume,  $\xi$  is the phase field variable,  $\phi$  is the electrostatic potential,  $\kappa_\xi$  is the gradient energy coefficient for the phase field,

$$\rho \equiv \mathcal{F} \sum_{j=1}^n z_j C_j \quad (6)$$

is the charge density,  $z_j$  is the valence of component  $j$  (equiv/mol or charge units per ion), and  $\mathcal{F}$  is Faraday's constant. The first term in the integral of Eq. (5) represents the energy density of a system without gradients and with no charge interactions; the second represents the gradient energy without electrostatic effects; and the third represents the electrostatic energy.

There are three constraints on the field variables of this system. The total number of moles  $n_j$  of each species  $j$  must be conserved over the volume  $V$

$$n_j = \int_V C_j dV = V \bar{C}_j, \quad j = 1 \dots n \quad (7)$$

where  $\bar{C}_j$  is the average concentration of species  $j$ . In addition, Eq. (4) and Poisson's equation

$$\nabla \cdot [\epsilon(\xi) \nabla \phi] + \rho = 0 \quad (8)$$

must be satisfied at every point in the system.  $\epsilon(\xi)$  is the electrical permittivity, whose value may depend on the phase.

We note that by invoking Poisson's equation (8), the electrostatic energy term in Eq. (5), given by  $\frac{1}{2} \rho \phi$ , could equivalently be represented as  $\frac{1}{2} \mathbf{D} \cdot \mathbf{E}$ , one half the scalar product of the displacement and the electric field of electromagnetic theory, or as  $\frac{\epsilon}{2} |\nabla \phi|^2$ . In this third form, we see that the electrostatic energy density is completely analogous to the phase field gradient energy density.

We perform a variational analysis on the resulting Lagrangian

$$\begin{aligned} \mathcal{L} = F - \int_V \lambda_V(\mathbf{x}) \left( \sum_{j=1}^n \bar{V}_j C_j - 1 \right) dV \\ - \sum_{j=1}^n \lambda_j \int_V (C_j - \bar{C}_j) dV \\ - \int_V \lambda_\phi(\mathbf{x}) \{ \nabla \cdot [\epsilon(\xi) \nabla \phi] + \rho \} dV \end{aligned} \quad (9)$$

where we have introduced the Lagrange multipliers  $\lambda_V(\mathbf{x})$ ,  $\lambda_j$ , and  $\lambda_\phi(\mathbf{x})$  for the constraints (4), (7), and (8) (note that the requirement that Eqs. (4) and (8) be satisfied everywhere in the system means that  $\lambda_V$  and  $\lambda_\phi$  must be fields). At equilibrium, each of the variations of  $\mathcal{L}$  must be independently zero,

$$\frac{\delta\mathcal{L}}{\delta C_j} = 0 = \frac{\partial f_V}{\partial C_j} + \frac{1}{2} \mathcal{F} z_j \phi - \lambda_j - \mathcal{F} z_j \lambda_\phi - \lambda_V \bar{V}_j \quad (10a)$$

$$j = 1 \dots n$$

$$\frac{\delta\mathcal{L}}{\delta\xi} = 0 = \frac{\partial f_V}{\partial\xi} - \kappa_\xi \nabla^2 \xi + \epsilon'(\xi) \nabla \lambda_\phi \nabla \phi \quad (10b)$$

$$\frac{\delta\mathcal{L}}{\delta\phi} = 0 = \frac{1}{2} \rho - \nabla \cdot [\epsilon(\xi) \nabla \lambda_\phi]. \quad (10c)$$

Using Poisson's equation to eliminate  $\rho$  in Eq. (10c), we determine that  $\lambda_\phi = -\phi/2$ . Here we have assumed that the natural boundary conditions  $0 = \partial\xi/\partial\mathbf{n} = \partial\phi/\partial\mathbf{n} = \partial\lambda_\phi/\partial\mathbf{n}$  hold on the boundary of  $V$ . Substituting this result into Eq. (10a),

$$\lambda_j = \frac{\partial f_V}{\partial C_j} + \mathcal{F} z_j \phi - \lambda_V(\mathbf{x}) \bar{V}_j. \quad j = 1 \dots n \quad (11)$$

Since  $\bar{V}_{e^-} = 0$  and  $\bar{V}_j = \bar{V}_s$  for all substitutional species, we can eliminate  $\lambda_V(\mathbf{x})$ .

We thus can summarize the equilibrium governing equations as

$$\begin{aligned} \lambda_{jn} &= \lambda_j - \frac{\bar{V}_j}{\bar{V}_s} \lambda_n \\ &= \left[ \frac{\partial f_V}{\partial C_j} + \mathcal{F} z_j \phi \right] - \frac{\bar{V}_j}{\bar{V}_s} \left[ \frac{\partial f_V}{\partial C_n} + \mathcal{F} z_n \phi \right] \\ &= \text{constant} \quad j = 1 \dots n-1 \end{aligned} \quad (12a)$$

$$0 = \frac{\partial f_V}{\partial\xi} - \kappa_\xi \nabla^2 \xi - \frac{\epsilon'(\xi)}{2} (\nabla \phi)^2 \quad (12b)$$

$$0 = \nabla \cdot [\epsilon(\xi) \nabla \phi] + \rho. \quad (12c)$$

It is convenient to identify the chemical potentials

$$\mu_j = \frac{\partial f_V}{\partial C_j} \quad j = 1 \dots n \quad (13)$$

and the electrochemical potentials

$$\bar{\mu}_j = \frac{\partial f_V}{\partial C_j} + \mathcal{F} z_j \phi, \quad j = 1 \dots n \quad (14)$$

such that Eq. (12a) becomes

$$\bar{\mu}_j - \frac{\bar{V}_j}{\bar{V}_s} \bar{\mu}_n = \text{constant}. \quad (15)$$

In Appendix A we show that, in one dimension,

$$\bar{\mu}_j = \bar{\mu}_j^\infty + \bar{V}_j \left( \frac{\kappa_\xi}{2} \xi_x^2 - \frac{\epsilon(\xi)}{2} \phi_x^2 \right), \quad j = 1 \dots n \quad (16)$$

where  $\bar{\mu}_j^\infty$  is the electrochemical potential far from the interface. First, we note that far from the interface, where  $\nabla\xi = \nabla\phi = 0$ , the value of the electrochemical potentials for each component  $j$  are identical in each phase, in agreement with Gibbsean thermodynamics [11]

$$\bar{\mu}_j^\alpha = \bar{\mu}_j^\beta. \quad j = 1 \dots n \quad (17)$$

Second, the electrochemical potential of  $e^-$  is uniform throughout the system. For the substitutional components, the electrochemical potential varies through the interface, even though the values in the bulk phases are equal. Because  $\nabla\phi = 0$  far from the interface, in the absence of external charges, Eq. (12c) requires that charge is zero in the bulk phases, such that

$$\sum_{j=1}^n z_j X_j^\alpha = \sum_{j=1}^n z_j X_j^\beta = 0. \quad (18)$$

### III. INTERFACIAL PROPERTIES

From electrocapillary theory [5], we know that surface energy  $\gamma$ , excess charge on the electrode  $\sigma^\alpha$ , and differential capacitance  $C_d$  are related by

$$\sigma^\alpha = - \left( \frac{\partial \gamma}{\partial \Delta\phi} \right)_{\mu_j} \quad (19)$$

$$C_d \equiv \left( \frac{\partial \sigma^\alpha}{\partial \Delta\phi} \right)_{\mu_j} = - \left( \frac{\partial^2 \gamma}{\partial \Delta\phi^2} \right)_{\mu_j} \quad (20)$$

where  $\Delta\phi = \phi^\alpha - \phi^\beta$  is the applied potential difference across the interface.<sup>1</sup> The potential in the electrolyte far from the interface is  $\phi^\beta$  and that in the electrode is  $\phi^\alpha$ . In a perfect conductor  $\phi^\alpha$  is uniform throughout the phase. The variation at constant chemical potential (constant concentration) is difficult to perform with physical electrode/electrolyte systems. In general, this variation can only be performed experimentally for an inert system such as a mercury electrode against an aqueous electrolyte. We seek to determine whether these relationships hold for our phase field model.

In Appendix B, we derive the expression for the surface energy

$$\gamma = \int_{-\infty}^{\infty} [\kappa_\xi \xi_x^2 - \epsilon(\xi) \phi_x^2] dx. \quad (21)$$

The first term in the integrand represents the contributions of the non-electrified interface. The second term is the contribution of electrostatics, such that the presence of electric fields always reduces the surface energy

<sup>1</sup> In classical electrochemistry, the actual difference in electrostatic potential across the interface is called the “inner” or “Galvani” potential difference.

from its charge-free value. In Appendix C we obtain the relationship

$$\sigma^\alpha = - \left( \frac{\partial \gamma}{\partial \Delta\phi^\circ} \right)_{\mu_j} \quad (22)$$

if  $\sigma^\alpha$  is defined by

$$\sigma^\alpha \equiv \int_{-\infty}^{\infty} p(\xi) \rho dx, \quad (23)$$

which is a completely reasonable definition of the surface charge on the electrode.  $p(\xi)$  is an interpolation function that will be described in Section IV A; in short,  $p(\xi) = 1$  in the electrode and  $p(\xi) = 0$  in the electrolyte. The notation  $\Delta\phi^\circ$  differs from that in Eqs. (19) and (20).  $\Delta\phi^\circ$  refers to a materials property of the electrode-electrolyte system, as we will discuss in Section IV B. Because we consider a non-inert electrode, we cannot vary the applied potential without affecting the concentration in the electrolyte. The variation considered in Eq. (22) is actually a variation with respect to a changing material property, rather than an applied potential. The differential capacitance is then defined to be

$$C_d \equiv \left( \frac{\partial \sigma^\alpha}{\partial \Delta\phi^\circ} \right)_{\mu_j}. \quad (24)$$

We note that a curved interface exhibits an additional relationship between surface energy, surface concentration, and the interfacial potential drop, consistent with the Gibbs-Thomson effect [12].

#### IV. THERMODYNAMIC FUNCTIONS AND MATERIAL PARAMETERS

To make the results of the phase field model more concrete and to permit numerical calculations, we must choose a particular form of the thermodynamic function and the materials parameters, at which point the model will be fully specified.

##### A. Choice of Form of the Thermodynamic Function

For simplicity, we assume that the chemical part of the Helmholtz free energy per unit volume is described by an ideal solution of the components.

$$\begin{aligned} f_V(\xi, C_1 \dots C_n) &= \frac{1}{V_m} f_m(\xi, X_1 \dots X_n) \\ &= \sum_{j=1}^n C_j \left\{ \mu_j^{\circ\alpha} p(\xi) + \mu_j^{\circ\beta} [1 - p(\xi)] \right. \\ &\quad \left. + RT \ln C_j V_m + W_j g(\xi) \right\} \quad (25) \end{aligned}$$

where  $\mu_j^{\circ\alpha}$  and  $\mu_j^{\circ\beta}$  are the chemical potentials of pure component  $j$  in the electrode (metal) phase and the electrolyte phase respectively,  $R$  is the molar gas constant, and  $T$  is the temperature. Following many phase field models of solidification [13], we use an interpolating function  $p(\xi) = \xi^3 (6\xi^2 - 15\xi + 10)$  to bridge between the descriptions of the two bulk phases and a double-well function  $g(\xi) = \xi^2 (1 - \xi)^2$  with a barrier height of  $W_j$  for each component  $j$  to establish the metal/electrolyte interface. The barrier heights  $W_j$  penalize interfaces which are too broad and the gradient energy coefficient  $\kappa_\xi$  penalizes interfaces which are too narrow. The polynomials are chosen to have the properties that  $p(0) = 0$ ,  $p(1) = 1$ ,  $p'(0) = p'(1) = 0$ , and  $p''(0) = p''(1) = 0$ . Other functions could be used.

For use in Eq. (12b), this free energy leads to

$$\frac{\partial f_V}{\partial \xi} = p'(\xi) \sum_{j=1}^n C_j \Delta\mu_j^\circ + g'(\xi) \sum_{j=1}^n C_j W_j, \quad (26)$$

where  $\Delta\mu_j^\circ \equiv \mu_j^{\circ\alpha} - \mu_j^{\circ\beta}$ .

The quantity  $\partial f_V / \partial C_j$  is also computed to give the electrochemical potentials,

$$\bar{\mu}_j = \mu_j^{\circ\beta} + \Delta\mu_j^\circ p(\xi) + RT \ln C_j V_m + z_j \mathcal{F} \phi + W_j g(\xi). \quad j = 1 \dots n \quad (27)$$

We note that the  $\bar{\mu}_j$  depend on all the  $C_j$  through the molar volume  $V_m$ .

##### B. Standard Chemical Potentials

We require values for the parameters  $\Delta\mu_j^\circ$  for each of the  $n$  species in our model in order to perform numerical calculations with the ideal solution thermodynamic model employed here. Given these numbers, we will know how the bulk electrode and electrolyte concentrations vary with the potential difference across the interface. From the equality of the bulk electrochemical potentials Eq. (17) and the ideal solution form of the electrochemical potential Eq. (27),

$$\Delta\phi = - \frac{\Delta\mu_j^\circ}{z_j \mathcal{F}} + \frac{RT}{z_j \mathcal{F}} \ln \frac{X_j^\beta}{X_j^\alpha}, \quad j = 1 \dots n \quad (28)$$

where the mole fractions are constrained by charge neutrality of the bulk phases Eq. (18) and the ordinary definition of the mole fractions Eq. (2).

One procedure to obtain information about the  $\Delta\mu_j^\circ$  is to specify one set of concentrations that are at equilibrium,  $X_j^{\alpha\circ}$  and  $X_j^{\beta\circ}$ . With such a set we can only determine three linear combinations of  $\Delta\mu_j^\circ$ . Given these three linear combinations, we cannot determine the potential difference across the interface, but we can calculate how the bulk electrode and electrolyte concentrations vary with changes in the potential difference across the

interface. In other words, the potential difference can only be described with respect to a reference electrode. Although knowledge of the potential difference between the phases is not necessary to describe the bulk equilibrium, it is necessary if one is interested in modeling the charge distribution between the electrode and electrolyte. We will designate  $\Delta\phi^\circ$  as the potential difference across the interface for the mole fractions  $X_j^{\alpha\circ}$  and  $X_j^{\beta\circ}$ , such that

$$\Delta\mu_j^\circ = RT \ln \frac{X_j^{\beta\circ}}{X_j^{\alpha\circ}} - z_j \mathcal{F} \Delta\phi^\circ. \quad j = 1 \dots n \quad (29)$$

Thus all four values of  $\Delta\mu_j^\circ$  can be computed. The quantity  $\Delta\phi^\circ$  is a material property that is fixed for a given choice of electrode and electrolyte system.

In traditional electrochemistry, one takes the reference mole fractions of the electroinactive species to be zero in one phase or the other, *e.g.*,  $X_{e^-}^{\circ\beta} = X_{A^-}^{\circ\alpha} = 0$ . One would then only equate the electrochemical potentials between the bulk phases of the electroactive species  $M^{+m}$  and  $N^{+n}$ . In this case it can be shown that

$$\mathcal{E}_{M^{+m}}^\circ - \mathcal{E}_{N^{+n}}^\circ = - \left( \frac{\Delta\mu_{M^{+m}}^\circ}{m\mathcal{F}} - \frac{\Delta\mu_{N^{+n}}^\circ}{n\mathcal{F}} \right), \quad (30)$$

where the standard potentials  $\mathcal{E}_{M^{+m}}^\circ$  are  $\mathcal{E}_{N^{+n}}^\circ$  are obtained from a table of electromotive series. Eq. (30) would be adequate to describe the concentration variations between the bulk phases.

For numerical purposes, we must assume small, but non-zero values for the reference concentrations of the electroinactive species, equivalent to assuming large (positive or negative), but finite, values for their standard potentials. In reality these concentrations are not zero, as might be indicated by an electrolyte with electronic conductivity or an electrode with some anion solubility [5, 14, 15].

In the remainder of the paper, we perform a detailed equilibrium analysis for an electrolyte where the component N has no charge, like an aqueous system ( $N = H_2O$ ) where dissociation of  $H_2O$  is neglected.<sup>2</sup> The lower density of charged species in an unsupported “aqueous” electrolyte allows us to resolve the equilibrium interface more accurately than in a system where all species can carry charge. Our paper on the dynamic behavior of the electrochemical phase field model [4] will treat the case of N with charge. The bulk standard state mole fractions are chosen for an electrode of M metal and an electrolyte of a solution containing 1 mol/L of  $M^{+2}$  and  $A^{-2}$  in a N solvent. We take the partial molar volume of the “substitutional” components ( $M^{+2}$ ,  $A^{-2}$ , and N) as that for pure water; *i.e.*,  $\bar{V}_s = 0.018 \text{ L/mol}$  or  $1/\bar{V}_s = 55.6 \text{ mol/L}$ . The voltage-independent portion

TABLE I: Numerical values of the potential-independent portion of the chemical potential differences  $\Delta\mu_j^\circ$ .

	$\ln(X_j^{\beta\circ}/X_j^{\alpha\circ})$
$e^-$	-13.41
$M^{+2}$	-2.919
$A^{-2}$	9.798
N	13.78

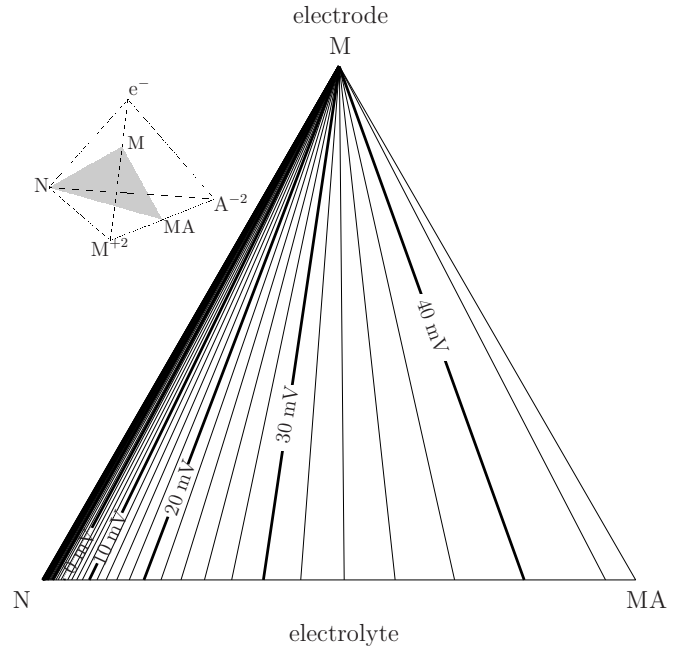


FIG. 1: Equilibrium phase diagram for the parameters in Table I. Tie-lines denote different values of the quantity  $(\Delta\phi - \Delta\phi^\circ)$ . The inset shows the position of this charge neutral phase diagram within the quaternary domain of the charged species.

of the chemical potential differences are given in Table I. The values for the electroinactive species are chosen to limit the corresponding standard state mole fractions to  $X_{e^-}^{\beta\circ} = X_{A^{-2}}^{\alpha\circ} = X_N^{\alpha\circ} = 10^{-6}$ .

Bulk charge neutrality can be invoked to transform the four mole fraction variables  $X_{e^-}$ ,  $X_{M^{+2}}$ ,  $X_{A^{-2}}$ , and  $X_N$  into mole fractions of three charge-neutral compounds,  $X_M \equiv \frac{3}{2}X_{e^-}$ ,  $X_{MA} \equiv 2X_{A^{-2}}$ , and  $X_N$ . We plot the equilibrium phase diagram in terms of these transformed mole fraction coordinates in Figure 1. Equilibrium states exist only between  $-0.0898 \text{ V} < \Delta\phi < +0.0427 \text{ V}$ . It can be seen that the electrode remains essentially pure M ( $X_{M^{+2}}^\alpha = 1/3$ ,  $X_{e^-}^\alpha = 2/3$ ) over the entire voltage range. At the lower  $\Delta\phi$  limit, the electrolyte is essentially pure N ( $X_N^\beta = 1$ ). At the upper  $\Delta\phi$  limit, the electrolyte is pure MA ( $X_{M^{+2}}^\beta = 1/2$ ,  $X_{A^{-2}}^\beta = 1/2$ ).

<sup>2</sup> The dissociation of  $H_2O$  could be handled by the addition of another component

### C. Other Parameters

A simplification, which should be eliminated in future work, is employed for the barrier height  $W_j$ . We set equal values for the substitutional species  $W_{j \in 2 \dots n} = W$ , and the value for the electrons,  $W_{e^-} = 0$ . This makes the last term in Eq. (26) independent of  $C_j$  and eliminates the  $W_j$  dependence in Eq. (12a).

In phase field models of solidification, where electrostatic effects are not included, the surface energy  $\gamma_\xi$  and the interfacial thickness  $\delta_\xi$  (of the  $\xi$ -field) are given by [16]

$$\gamma_\xi = \sqrt{\frac{\kappa_\xi W}{18\bar{V}_s}} \quad (31)$$

$$\delta_\xi = \sqrt{\frac{\kappa_\xi \bar{V}_s}{2W}}. \quad (32)$$

We include the subscript  $\xi$  with the realization that there will be an electrostatic contribution to the surface energy (see Eq. (21)) and an independent electrostatic length scale. For numerical calculations, we choose the approximate values of  $\gamma_\xi = 0.2 \text{ J/m}^2$  and  $\delta_\xi = 3 \times 10^{-11} \text{ m}$ , which give  $W = 3.6 \times 10^5 \text{ J/mol}$  and  $\kappa_\xi = 3.6 \times 10^{-11} \text{ J/m}$ . We defer the complications of a phase-dependent permittivity to future studies and take  $\epsilon(\xi) = 78.49\epsilon_0$ , where  $\epsilon_0$  is the permittivity of free space. This is the value typically cited for an aqueous electrolyte [5].

## V. NUMERICAL METHODS

Numerical solutions to the governing equations Eq. (12) were obtained by both a relaxation method and a pseudo-spectral technique on a one-dimensional domain of length  $L$ . The relaxation method had the advantages that it was simple to code and would eventually converge to a solution even from a step-function initial condition. The main disadvantage of the technique is that it is very slow. Run times of several hours to several days were needed to reach convergence on a 1.6 GHz AMD Athlon running Debian GNU/Linux v3.0 with a 2.4 kernel and using the Portland Group pgcc compiler.<sup>3</sup> In contrast, the pseudo-spectral technique can produce solutions in a few minutes, but only from a very good initial guess.

<sup>3</sup> Certain commercial products are identified in this paper in order to adequately specify procedures being described. In no case does such identification imply recommendation or endorsement by the National Institute of Standards and Technology, nor does it imply the material identified is necessarily the best for the purpose.

TABLE II: Boundary Conditions

electrode ( $x = 0$ )	electrolyte ( $x = L$ )
$\mathbf{n} \cdot \nabla \xi = 0$	$\mathbf{n} \cdot \nabla \xi = 0$
$\phi = 0$	$\mathbf{n} \cdot \nabla \phi = 0$
$C_j$ specified	$C_j$ specified

### A. Relaxation

Relaxation solutions [17] to Eq. (12) were obtained by casting the equilibrium ordinary differential equations (12a) and (12b) as the time dependent partial differential equations

$$\frac{\partial C_j}{\partial t} = \nabla \cdot \left\{ M_j \nabla \frac{\delta \mathcal{L}}{\delta C_j} \right\} = \nabla \cdot \left\{ M_j \nabla \left[ \bar{\mu}_j - \frac{\bar{V}_j}{V_n} \bar{\mu}_n \right] \right\} \quad (33a)$$

$$j = 1, \dots, n-1$$

and

$$\frac{\partial \xi}{\partial t} = -M_\xi \frac{\delta \mathcal{L}}{\delta \xi} = -M_\xi \left[ \frac{\partial f_V}{\partial \xi} - \kappa_\xi \nabla^2 \xi - \frac{\epsilon'(\xi)}{2} (\nabla \phi)^2 \right], \quad (33b)$$

where  $t$  is time,  $M_j$  is the mobility of component  $j$ , and  $M_\xi$  is the mobility of the phase field. We defer discussion of the mobilities  $M_\xi$  and  $M_j$  to our paper on kinetics [4] as their values are not important to the present analysis of electrochemical equilibrium. Equations (33) are the simplest expressions that guarantee a decrease in total free energy with time. Poisson's equation (12c) must still be satisfied everywhere. Equations (12c) and (33) were solved with explicit finite differences. Spatial derivatives were taken to second order on a uniform mesh. Solutions were integrated to equilibrium with an adaptive, fifth-order Runge-Kutta time stepper [17]. We defined equilibrium as the point when Eqs. (12a) and (A6) were satisfied to within 0.1%.

Simulations were started with an abrupt interface between the bulk electrode and electrolyte phases, such that  $\xi^\alpha = 1$  and  $\xi^\beta = 0$ . After choosing a value for  $C_{\text{M}^+}^\beta$ , the remaining bulk  $C_j$  were determined from Figure 1. Because  $\rho = 0$  for the bulk concentrations, Eq. (12c) gives  $\nabla \phi = 0$  throughout the domain for the initial data. The boundary conditions are listed in Table II.

### B. Adaptive pseudospectral discretization

In order to increase the numerical resolution of the interfacial region, we have also employed an adaptive solution technique based on a spectral approximation [18] to the governing equations (12). To reduce the number of unknowns in the system, we eliminate the solute variables by solving the governing equations (12a), together with the constraint equation (4). Given values of  $\xi$  and

$\phi$  at a point, this provides an algebraic form for the solute fields  $C_j$  at this point. The remaining equations (12b) and (12c) are discretized using a pseudospectral formulation of a spectral element representation of the second derivative [19]. It is convenient to fix the interface location by specifying  $\xi(x_I) = 1/2$  at a given grid point  $x_I$ . The discretization procedure then provides a set of nonlinear equations with an equal number of unknowns. The nonlinear equations are solved using the quasi-Newton software package SNSQ [20]. Starting estimates for the solution procedure are generally obtained by continuation from the finite difference procedure described above, or from previous pseudospectral solutions.

An adaptive procedure is obtained by bisecting the elements for which an error estimate indicates that additional refinement is necessary. The error estimate is based on the rate of decay of a Chebyshev expansion of the solution components; a simple criterion is based on requiring the magnitude of the last two coefficients of the charge density in each panel to lie below a given threshold. If a refinement is necessary, the element is bisected and the previous solution is interpolated to the nodes of the new panels. The nonlinear equations are then solved on the new nodes, and the procedure is repeated until each Chebyshev expansion has rapid decay, indicating that the solution is well-resolved on each panel. Since the previous solution provides a good starting guess, the successive solutions converge quickly, and the overall run time is a small multiple of the time required for a single solution step on a grid with equal pseudospectral elements.

## VI. NUMERICAL RESULTS

Figure 2 shows plots of phase field, voltage and charge across the interface for  $\Delta\phi^\circ = (-0.1, 0, +0.1)$  V obtained using the relaxation method in 1D over a domain 3.2 nm long and containing 1200 mesh points. The tick marks at the top of Figure 2(a) indicate the positions of the mesh points used in the two different solution methods. The relaxation and pseudospectral calculations have a linear correlation of 0.9992 for the most sensitive field  $\rho$ ; the other fields have a linear correlation of 0.9999 or better.

Figure 2 focuses on the interface region of this computational domain. The bulk concentration of  $M^+$  and  $A^-$  in the electrolyte is 0.25 mol/L. The variation of  $\xi$  between the electrode on the left and the electrolyte on the right for the three cases is virtually identical. A fit of all three curves to  $\xi(x) = \{1 - \tanh[(x - x_0)/2\delta_\xi]\}/2$  gives  $\delta_\xi = (2.480 \pm 0.009) \times 10^{-11}$  m, which compares well with the value we assumed in Section IV C.  $\xi$  changes from 0.9 to 0.1 over a distance of approximately 0.1 nm or  $4\delta_\xi$ . This represents the thickness of the electrode-electrolyte interface. The voltage  $\phi$  changes smoothly between a value of zero in the electrode (as assumed) to an asymptotic value in the electrolyte far from the interface equal to  $(RT/2\mathcal{F}) \ln[(1 \text{ mol/L})/(0.25 \text{ mol/L})] - \Delta\phi^\circ$ .

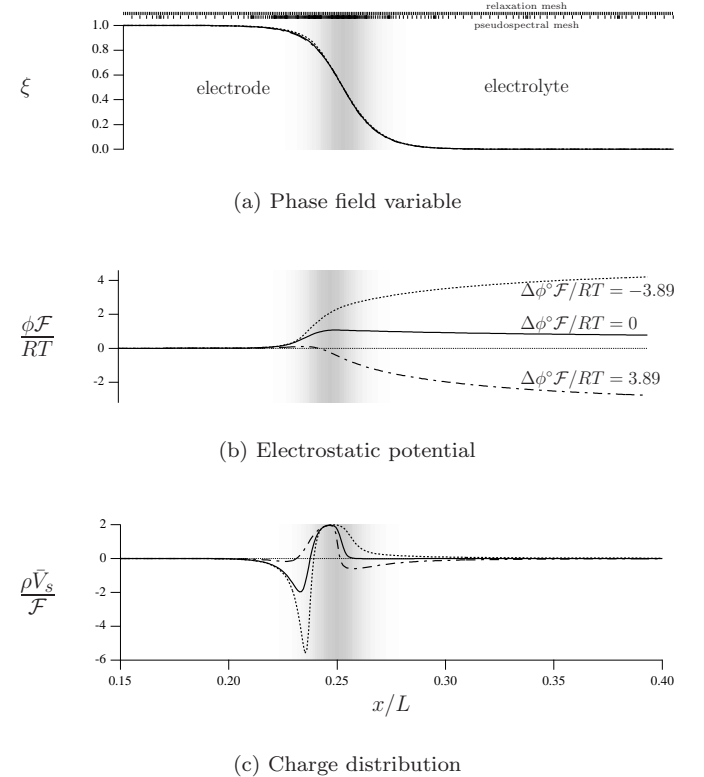


FIG. 2: Profiles through the interface for  $\Delta\phi^\circ = -0.1$  V, 0 V, and  $+0.1$  V.  $g(\xi)$  is mapped onto the background in gray to indicate the location of the interface. The ticks marks at the top of Figure 2(a) indicate the positions of the mesh points for the two different solution methods.

The charge  $\rho$ , while zero far from the interfacial region, exhibits a distinct charge separation within the interfacial region. The charge distribution is quite different for the three cases. For  $\Delta\phi^\circ = -0.1$  V and 0.0 V, a negative charge is present to the left. For  $\Delta\phi^\circ = +0.1$  V, the negative charge is to the right. Figure 3 shows the variation in the concentrations from the electrode to the electrolyte. The values at the ends of the full computational domain correspond to a bulk M electrode, a 0.25 mol/L MA in N electrolyte, with impurities as allowed by Table I. The abrupt change in concentrations through the distance where  $\xi$  is changing is followed by a more gradual change in the electrolyte. The gradual concentration decay length in the electrolyte is the same as that of the voltage. One could define the surface excess as the difference between the actual concentration and some interpolation between the bulk values and see that there is an adsorption of the different species at the interface which depends on the value of  $\Delta\phi^\circ$ .

In Appendix D we summarize the Gouy-Chapman-Stern model of the double layer. That treatment predicts an exponential decay of the potential in the electrolyte away from the electrode, with a decay length of  $\delta_\phi^{GC}$ . Figure 4 shows a fit of the  $\phi$  vs. distance plots from Fig-

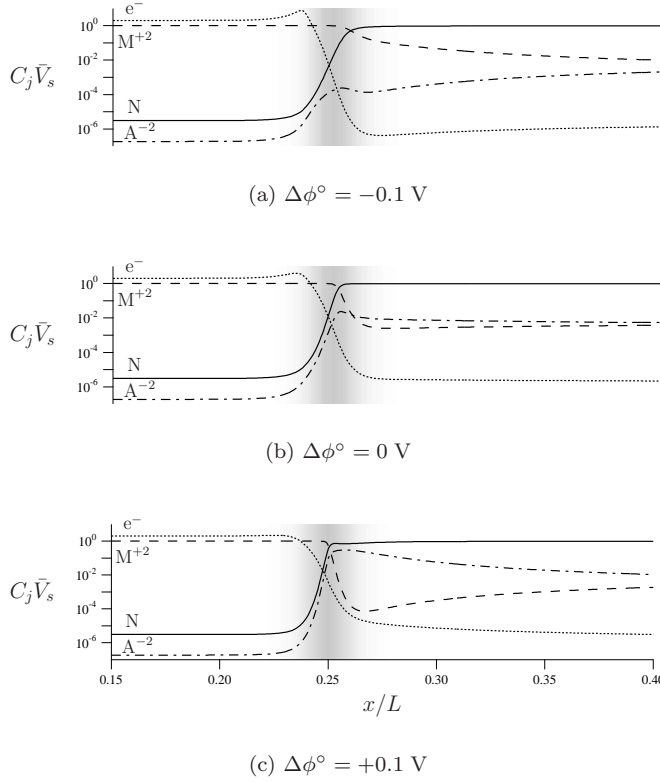


FIG. 3: Concentration profiles through the interface for different values of  $\Delta\phi^\circ$ .  $g(\xi)$  is mapped onto the background in gray to indicate the location of the interface.

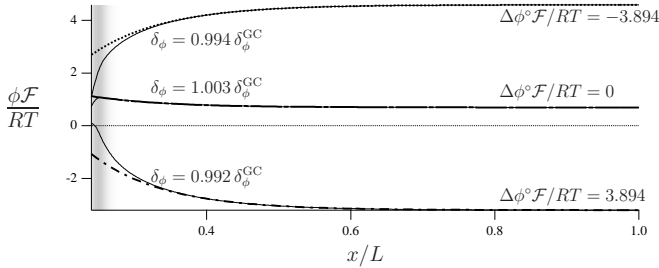


FIG. 4: Exponential fits (heavy dashed lines) to potential curves of Figure 2(b) (light solid lines).  $g(\xi)$  is mapped onto the background in gray to indicate the location of the interface.

ure 2(b) to  $\phi = \phi_\infty + (\phi_0 - \phi_\infty) \exp(-x/\delta_\phi)$ . The fit is excellent. The decay length  $\delta_\phi$  of  $\phi$  to its asymptotic value is very close to the predicted value of  $\delta_\phi^{\text{GC}}$ . This length is over ten times larger than  $\delta_\xi$  and approximately three times the apparent interface thickness.

Figure 5(a) shows the surface energy (from Eq. (21)) vs.  $\Delta\phi^\circ$  and Figure 5(b) shows a plot of  $\sigma^\alpha$  vs.  $\Delta\phi^\circ$ , both obtained by the two numerical methods. The point of zero charge (PZC), defined by  $\sigma^\alpha = \sigma^\beta = 0$ , occurs at  $\Delta\phi^\circ = +0.005$  V for 1 mol/L and  $\Delta\phi^\circ = +0.035$  V for 0.25 mol/L. At the point of zero charge,  $\rho$  is not con-

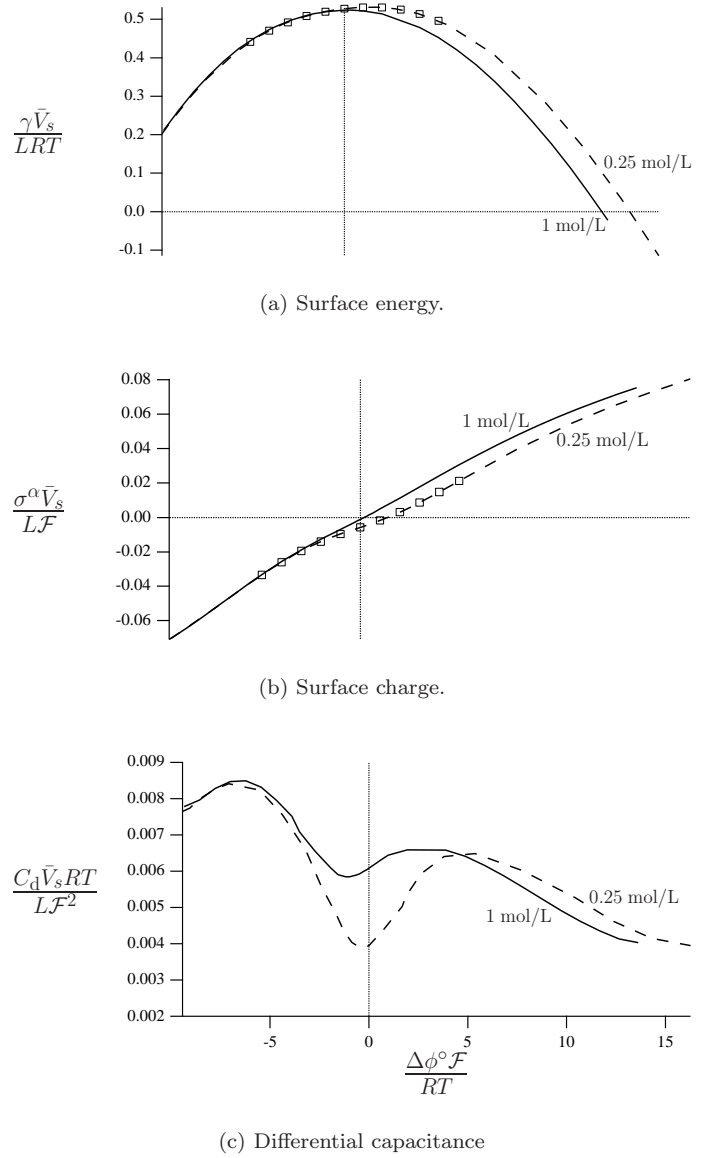


FIG. 5: Interface properties as functions of  $\Delta\phi^\circ$ . Open symbols are calculated by the relaxation method of Section V A. Lines are calculated by the pseudospectral method of Section V B.

stant, nor is the electrostatic potential, but rather, the integrated charge is zero in each phase and there is some potential step between them. We note that Grahame described exactly this condition in his seminal paper on the electrochemical double-layer [5]. The presence of dipoles at the interface guarantees that the potential will not be uniform. The surface charge curve shows a slight deviation from linearity away from the point of zero charge. This dome shaped curve in Figure 5(a) has a maximum surface energy of approximately 0.225 J/m<sup>2</sup> at a value of  $\Delta\phi^\circ = +0.005$  V, the point of zero charge. This maximum surface energy value is very close to  $\gamma_\xi$ , used to

establish numerical values for  $W$  and  $\kappa_\xi$ . Figures 5(a) and 5(b) obey Eq. (19) very closely. The negative surface energies obtained for large positive values of  $\Delta\phi^\circ$  indicate that a planar interface will become unstable to perturbations which increase surface area. Such perturbations are not possible given the symmetry constraints of our 1D solutions, but attention will need to be paid to this when higher dimensional calculations are performed.

From Eq. (20), the differential capacitance is obtained as the derivative of Figure 5(b) with respect to  $\Delta\phi^\circ$ . The relaxation method used to produce the open square points in Figure 5(b) is not fast enough to allow calculating a numeric derivative of sufficient resolution. We thus use the results of the spectral method, which can compute with a much greater resolution and over a wider range of  $\Delta\phi^\circ$ , to calculate Figure 5(c).

Our calculated differential capacitance curve, replotted in Figure 6(a), does not resemble the hyperbolic cosine predicted by the Gouy-Chapman theory ( $x_2 = 0$  in Eq. (D5)), shown in Figure 6(b). Neither does it resemble the truncated hyperbolic cosine predicted by the Gouy-Chapman-Stern theory ( $x_2 \neq 0$  in Eq. (D5)), shown in Figure 6(c) (we take  $\epsilon/x_2 = 5 \text{ F/m}^2$  for illustration only). On the other hand, it does bear a striking resemblance to experimental differential capacitance curves [5, 9, 10], such as Valette and Hamelin's measurements of Ag electrodes in NaF solutions, shown in Figure 6(d).

## VII. DISCUSSION AND CONCLUSIONS

This paper has explored the equilibrium structure of an electrified interface between two phases consisting of charged components, as described by a phase field model. Such a model, being a continuum description, adds only the bare essentials of the physics and chemistry of electrochemical interfaces: mass and volume constraints, Poisson's equation, ideal solution thermodynamics in the bulk, and a simple description of the competing energies in the interface. Despite this simple description, the model realizes the oft described behavior of the double layer; namely, the charge separation at the interface and its dependence on voltage drop (Galvani or inner potential) across the interface. As the Galvani potential is varied at constant compositions of the electrode and electrolyte (constant chemical potentials), the model reproduces the well known maximum of the surface energy curve at the point of zero surface charge (PZC). High precision pseudospectral solutions of the governing equations also deliver differential capacitance variations with Galvani potential that exhibit much more complex and realistic behavior than do the simple Gouy-Chapman-Stern models. The full range of behavior encompassed by the model must await further research. For example, the effect of unequal and/or nonzero barrier heights  $W_j$  for the components will surely affect the adsorption and, in turn, the surface energy and capacitance curves.

A recent lattice-gas model of an electrochemical sys-

tem [21, 22] exhibits interfacial structures very similar to those found in this paper. That model also demonstrates simple dendrites during plating, but those lattice-gas papers do not explore the electrocapillary behavior discussed in this paper. The similarities of the predictions between that discrete model and our continuum approach may permit a bridge between atomistic treatments of the electrochemical interface and macroscopic descriptions of electroplating.

To model a real electrochemical system with this method, one needs to match the parameters of the phase field model to the experimentally determined (or the normally applied) understanding of the particular electrochemical system. In addition to kinetic parameters described in Ref. [4], equilibrium solutions require several pieces of information. At a minimum one requires:

1. a description of the bulk thermodynamics of the electrode and electrolyte,
2. the dielectric constant of the electrolyte and electrode,
3. an estimate for the physical thickness of the electrode / electrolyte phase interface,
4. the actual (Galvani) potential across the interface for some concentration of co-existing electrolyte and electrode phases, and
5. the surface energy *or* the capacitance of the interface for these concentrations.

Although we currently lack an analytical expression for the relation between the phase field parameters  $\kappa_\xi$  and  $W_j$  and the information in 3 and 5 above, the numerical results of the paper show that they are connected. In the future, an asymptotic analysis of the governing equations may reveal these relationships directly. Finally, the non-ideal solution behavior of the electrolyte, which may involve complexing of ions, should be addressed. Concentration would be replaced by presumably known activity coefficients.

Solution of the governing equations has proved difficult. The resolution of the charge through the interfacial region requires many more mesh points than typical of phase field models of solidification of binary alloys. This is due to the more intricate structure of the charge distribution in the interface as compared to the structure of the phase and concentration fields. An adaptive solution method, which concentrates mesh points in this interfacial region, permits significantly improved calculation speed.

## Acknowledgments

J. W. Cahn, S. Coriell, A. Lobkovsky, R. F. Sekerka, and D. Wheeler have been very helpful with our formulation and coding of the phase field model. We have learned

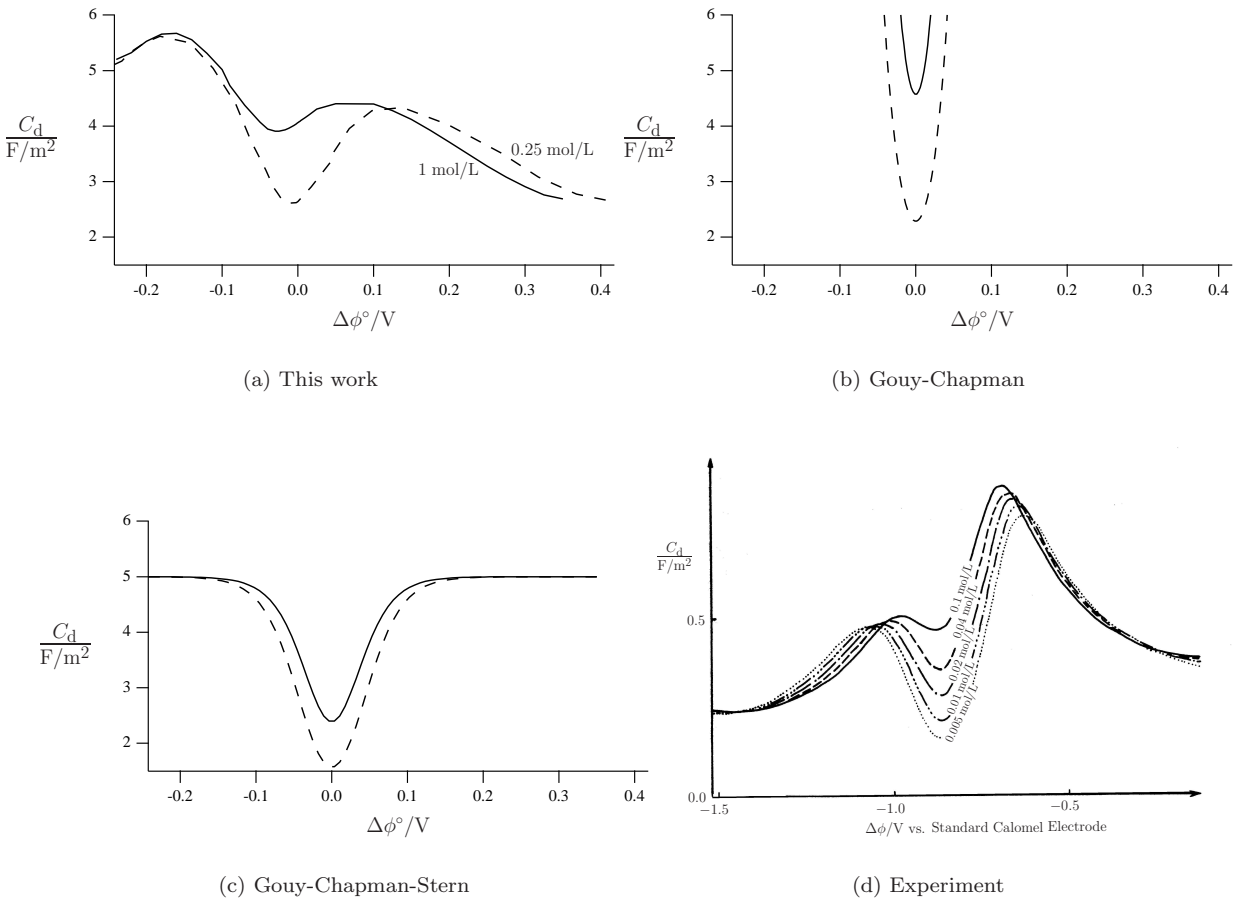


FIG. 6: Comparison of the differential capacitance results of this model with the predictions of the sharp interface theories outlined in Appendix D and the experimental measurements of Ag(100) electrodes in aqueous solutions of NaF [Reprinted from *J. Electroanal. Chem.* **138**, G. Valette, “Double layer on silver single crystal electrodes in contact with electrolytes having anions which are slightly specifically adsorbed Part II. The (100) face”, 37–54, Copyright (1982), with permission from Elsevier].

a significant amount about electrochemistry through discussions with U. Bertocci, E. Gileadi, T. P. Moffat, and G. R. Stafford. This manuscript benefited from a critical

reading by E. García. Part of this research was supported by the Microgravity Research Division of NASA.

---

[1] D. Josell, D. Wheeler, and W. H. Huber, *Phys. Rev. Lett.* **87**, 016102 (2001).

[2] W. J. Boettinger, J. A. Warren, C. Beckermann, and A. Karma, *Annu. Rev. Mater. Res.* **32**, 163 (2002).

[3] G. B. McFadden, *Contemporary Mathematics* **306**, 107 (2002).

[4] J. E. Guyer, W. J. Boettinger, J. A. Warren, and G. B. McFadden, *Phase field modeling of electrochemistry: Kinetics*, unpublished.

[5] D. C. Grahame, *Chem. Rev.* **41**, 441 (1947).

[6] K. J. Vetter, *Electrochemical Kinetics: Theoretical and Experimental Aspects* (Academic Press Inc., New York, 1967).

[7] J. O. Bockris, A. K. N. Reddy, and M. Gamboa-Aldeco, in *Modern Electrochemistry* (Kluwer Academic/Plenum Publishers, New York, 2000), vol. 2A.

[8] A. J. Bard and L. R. Faulkner, *Electrochemical Methods: Fundamentals and Applications* (John Wiley & Sons, Inc., New York, 2001).

[9] G. Valette and A. Hamelin, *Electroanal. Chem. Interf. Electrochem.* **45**, 301 (1973).

[10] G. Valette, *J. Electroanal. Chem.* **138**, 37 (1982).

[11] J. W. Gibbs, *The Scientific Papers of J. Willard Gibbs* (Longmans, Green, and Co., London, 1906).

[12] G. B. McFadden, *Electrochemical Gibbs-Thomson effect*, unpublished research.

[13] S.-L. Wang, R. Sekerka, A. A. Wheeler, B. T. Murray, S. R. Coriell, R. J. Braun, and G. B. McFadden, *Physica D* **69**, 189 (1993).

[14] E. J. Hart and J. W. Boag, *J. Amer. Chem. Soc.* **84**, 4090 (1962).

[15] J. J. Egan and W. Freyland, *Ber. Bunsenges. Phys.*

Chem. **89**, 381 (1985).

[16] A. A. Wheeler, W. J. Boettinger, and G. B. McFadden, Phys. Rev. A **45**(10), 7427 (1992).

[17] W. H. Press, S. A. Teukolsky, W. T. Vetterling, and B. P. Flannery, *Numerical Recipes in C: the Art of Scientific Computing* (Cambridge University Press, 1999), 2nd ed.

[18] D. Gottlieb, M. Y. Hussaini, and S. A. Orszag, in *Spectral Methods for Partial Differential Equations*, edited by R. G. Voigt, D. Gottlieb, and M. Y. Hussaini (SIAM, Philadelphia, 1984), pp. 1–54.

[19] A. T. Patera, J. Comp. Phys. **54**, 468 (1984).

[20] K. L. Hiebert, SLATEC *Common Math Library*, National Energy Software Center, Argonne National Laboratory, Argonne, IL (1980), based on Powell [23].

[21] M.-O. Bernard, M. Plapp, and J.-F. Gouyet, in *Complexity and Fractals in Nature*, edited by M. M. Novak (World Scientific, Singapore, 2001), pp. 235–246.

[22] M.-O. Bernard, M. Plapp, and J.-F. Gouyet, *A mean-field kinetic lattice gas model of electrochemical cells* (2003), cond-mat/0303072v1.

[23] M. J. D. Powell, in *Numerical Methods for Nonlinear Algebraic Equations*, edited by P. Rabinowitz (Gordon and Breach, New York, NY, 1970), pp. 87–161.

[24] J. W. Cahn, in *Interfacial Segregation*, edited by W. C. Johnson and J. M. Blakely (ASM, Metals Park, OH, 1979), pp. 3–23.

## APPENDIX A: FIRST INTEGRAL

Here we characterize a first integral of the steady-state one-dimensional equilibrium equations, and use it to obtain an expression for the surface energy  $\gamma$ .

It is convenient to introduce the electrochemical free energy density

$$\bar{f}_V(\xi, C_1 \dots C_n, \phi) = \sum_{j=1}^n C_j \bar{\mu}_j(\xi, C_1 \dots C_n, \phi). \quad (\text{A1})$$

Here  $\bar{\mu}_j = \mu_j + z_j \mathcal{F}\phi = \partial \bar{f}_V / \partial C_j$  is the electrochemical potential of species  $j$ , and the charge density is given by  $\rho = \partial \bar{f}_V / \partial \phi$ . The steady-state one-dimensional equilibrium equations can then be written compactly in terms of  $\bar{f}_V$ , and assume the form

$$\bar{\mu}_j - \frac{\bar{V}_j}{V_s} \bar{\mu}_n = \lambda_{jn}, \quad j = 1 \dots n-1 \quad (\text{A2a})$$

$$\frac{\partial \bar{f}_V}{\partial \xi} - \kappa_\xi \xi_{xx} - \frac{\epsilon'(\xi)}{2} \phi_x^2 = 0, \quad (\text{A2b})$$

$$\frac{\partial \bar{f}_V}{\partial \phi} + (\epsilon(\xi) \phi_x)_x = 0. \quad (\text{A2c})$$

If we differentiate the electrochemical free energy density of the equilibrium solution with respect to  $\xi(x)$ ,

$C_j(x)$ , and  $\phi(x)$ , we find

$$\begin{aligned} & \frac{d}{dx} \bar{f}_V(\xi(x), C_1(x) \dots C_n(x), \phi(x)) \\ &= \frac{\partial \bar{f}_V}{\partial \xi} \xi'(x) + \sum_{j=1}^n \frac{\partial \bar{f}_V}{\partial C_j} C'_j(x) + \frac{\partial \bar{f}_V}{\partial \phi} \phi'(x) \\ &= \xi'(x) \left[ \kappa_\xi \xi_{xx} + \frac{\epsilon'(\xi)}{2} \phi_x^2 \right] \\ & \quad + \sum_{j=1}^{n-1} \left[ \bar{\mu}_j - \frac{\bar{V}_j}{V_s} \bar{\mu}_n \right] C'_j(x) - \phi'(x) (\epsilon(\xi) \phi_x)_x, \end{aligned} \quad (\text{A3})$$

where we have used the volume constraint Eq. (4) and the governing equations (A2) to eliminate the partial derivatives of  $\bar{f}_V$ . This expression can be simplified to give

$$\begin{aligned} & \frac{d}{dx} \left[ \bar{f}_V(\xi(x), C_1(x) \dots C_n(x), \phi(x)) \right. \\ & \quad \left. - \sum_{j=1}^{n-1} \lambda_{jn} C_j - \frac{\kappa_\xi}{2} \xi_x^2 + \frac{\epsilon(\xi)}{2} \phi_x^2 \right] = 0. \quad (\text{A4}) \end{aligned}$$

Since, from Eqs. (4) and (A1) we have

$$\begin{aligned} & \bar{f}_V(\xi(x), C_1(x) \dots C_n, \phi(x)) \\ &= \sum_{j=1}^{n-1} \left[ \bar{\mu}_j - \frac{\bar{V}_j}{V_s} \bar{\mu}_n \right] C_j + \frac{\bar{\mu}_n}{V_s} \\ &= \sum_{j=1}^{n-1} \lambda_{jn} C_j + \frac{\bar{\mu}_n}{V_s}, \end{aligned} \quad (\text{A5})$$

we may write the first integral represented by Eq. (A4) in the form

$$\frac{\bar{\mu}_n}{V_s} - \frac{\kappa_\xi}{2} \xi_x^2 + \frac{\epsilon(\xi)}{2} \phi_x^2 = \text{constant} = \frac{\bar{\mu}_n^\infty}{V_s}, \quad (\text{A6})$$

where we have evaluated the integration constant in the far field where  $\xi_x = \phi_x = 0$  and  $\bar{\mu}_n = \bar{\mu}_n^\infty$ . In view of Eq. (A2a), we therefore find that the electrochemical potentials of the substitutional species vary through the interface, with

$$\bar{\mu}_j = \bar{\mu}_j^\infty + \bar{V}_j \left( \frac{\kappa_\xi}{2} \xi_x^2 - \frac{\epsilon(\xi)}{2} \phi_x^2 \right). \quad j = 1 \dots n \quad (\text{16})$$

The interstitial species, with  $\bar{V}_j = 0$ , thus have uniform electrochemical potentials.

An alternative form of the free energy functional of

Eq. (5) takes the form <sup>4</sup>

$$F(\xi, C_1 \dots C_n, \phi) = \int_V \left[ \bar{f}_V(\xi, C_1 \dots C_n, \phi) + \frac{\kappa_\xi}{2} |\nabla \xi|^2 - \frac{\epsilon(\xi)}{2} |\nabla \phi|^2 \right] dV. \quad (\text{A7})$$

## APPENDIX B: SURFACE ENERGY

A conventional definition of the surface energy  $\gamma$  of a planar interface at equilibrium between two isothermal, multicomponent, fluid phases, with no electrical effects or volume constraints, is to write [24]

$$F = \sum_{j=1}^n \mu_j^\infty n_j - P^\infty V + \gamma A, \quad (\text{B1})$$

where  $P^\infty$  is the far field value of the pressure  $P$ . The interface is located in the interior of the region  $-L/2 < x < L/2$  and the free energy is

$$F = A \int_{-L/2}^{L/2} f_V dx = A \int_{-L/2}^{L/2} \left( \sum_{j=1}^n \mu_j C_j - P \right) dx. \quad (\text{B2})$$

In our model of the electrolyte-electrode equilibrium, we are neglecting the pressure term in Eqs. (B1) and (B2), and including a volume constraint and the effects of an electric field on charged components. The appropriate definition of  $\gamma$  is analogous to Eq. (B1), with

$$F = \sum_{j=1}^n \bar{\mu}_j^\infty n_j + \gamma A, \quad (\text{B3})$$

and  $n_j$  is defined by Eq. (7). The surface energy arises from the variation in the substitutional electrochemical potentials across the interface. From Eq. (A7)

$$\gamma = \int_{-L/2}^{L/2} \left[ \bar{f}_V - \sum_{j=1}^n \bar{\mu}_j^\infty C_j + \frac{\kappa_\xi}{2} \xi_x^2 - \frac{\epsilon(\xi)}{2} \phi_x^2 \right] dx \quad (\text{B4})$$

On substitution of Eqs. (A1) and (16) into Eq. (B4) we obtain

$$\gamma = \int_{-L/2}^{L/2} [\kappa_\xi \xi_x^2 - \epsilon(\xi) \phi_x^2] dx. \quad (\text{B1})$$

## APPENDIX C: SURFACE CHARGE AND CAPACITANCE

Here we derive the expression (19) for the variation in surface energy  $\gamma$  associated with changes in the Galvani potential  $\Delta\phi^\circ$  under the assumption of ideal solution thermodynamics (Eq. (25)). The derivation can be generalized to non-ideal solution behavior if activity coefficients are introduced. The variation is computed for fixed values of the far-field mole fractions  $X_j^\alpha$  and  $X_j^\beta$ , so that from Eqs. (27) and (29) we see that the variation  $\delta\Delta\phi^\circ$  then induces corresponding variations  $\delta\Delta\mu_j^\circ = -z_j \mathcal{F} \delta\Delta\phi^\circ$  and the related expression  $\delta\bar{\mu}_j^\infty = -z_j \mathcal{F} \delta\Delta\phi^\circ$ . The variation in  $\Delta\phi^\circ$  also leads to variations  $\delta\phi(x)$ ,  $\delta C_j(x)$ , and  $\delta\xi(x)$  in the equilibrium profiles of the field variables as well. We compute the resulting variation of the surface energy,  $\delta\gamma$ .

From Eq. (B4) we have

$$\delta\gamma = \int_{-L/2}^{L/2} \left[ \delta\bar{f}_V - \sum_{j=1}^n \bar{\mu}_j^\infty \delta C_j - \sum_{j=1}^n C_j \delta\bar{\mu}_j^\infty + \kappa_\xi \xi_x \delta\xi_x - \epsilon(\xi) \phi_x \delta\phi_x - \frac{\epsilon'(\xi)}{2} \phi_x^2 \delta\xi \right] dx. \quad (\text{C1})$$

In computing the variation  $\delta\bar{f}_V$ , we must consider not only the explicit variations arising from  $\delta\phi(x)$ ,  $\delta C_j(x)$ , and  $\delta\xi(x)$ , but also take into account the implicit variation associated with the dependence of  $\bar{f}_V$  on  $\Delta\mu_j^\circ$ . We then find

$$\begin{aligned} \delta\bar{f}_V &= \frac{\partial\bar{f}_V}{\partial\xi} \delta\xi(x) + \sum_{j=1}^n \frac{\partial\bar{f}_V}{\partial C_j} \delta C_j \\ &+ \frac{\partial\bar{f}_V}{\partial\phi} \delta\phi(x) + \sum_{j=1}^n \frac{\partial\bar{f}_V}{\partial\Delta\mu_j^\circ} \delta\Delta\mu_j^\circ \end{aligned} \quad (\text{C2})$$

$$\begin{aligned} &= \frac{\partial\bar{f}_V}{\partial\xi} \delta\xi(x) + \sum_{j=1}^n \bar{\mu}_j \delta C_j \\ &+ \frac{\partial\bar{f}_V}{\partial\phi} \delta\phi(x) - p(\xi) \rho(x) \delta\Delta\phi^\circ, \end{aligned} \quad (\text{C3})$$

where we have used  $\partial\bar{f}_V/\partial\Delta\mu_j^\circ = C_j p(\xi)$  and  $\delta\Delta\mu_j^\circ = -z_j \mathcal{F} \delta\Delta\phi^\circ$ . Inserting this expression into Eq. (C1) and integrating by parts, we find

$$\begin{aligned} \delta\gamma &= \int_{-L/2}^{L/2} \left\{ \left[ \frac{\partial\bar{f}_V}{\partial\xi} - \kappa_\xi \xi_{xx} - \frac{\epsilon'(\xi)}{2} \phi_x^2 \right] \delta\xi \right. \\ &+ \sum_{j=1}^n (\bar{\mu}_j - \bar{\mu}_j^\infty) \delta C_j - \sum_{j=1}^n C_j \delta\bar{\mu}_j^\infty \\ &\left. + \left[ \frac{\partial\bar{f}_V}{\partial\phi} + (\epsilon(\xi) \phi_x)_x \right] \delta\phi - p(\xi) \rho(x) \delta\Delta\phi^\circ \right\} dx. \end{aligned} \quad (\text{C4})$$

<sup>4</sup> Here we have used the identity  $\int \rho\phi dx = \int \epsilon(\xi) \phi_x^2 dx$ , which follows from the Poisson equation with appropriate boundary conditions.

Using the equilibrium equations (A2), Eq. (16),  $\delta\bar{\mu}_j^\infty = z_j\mathcal{F}\delta\Delta\phi^\circ$ , and  $\sum_{j=1}^n \bar{V}_j\delta C_j = 0$  (which follows from Eq. (4)), to simplify the results, we obtain

$$\delta\gamma = \delta\Delta\phi^\circ \int_{-L/2}^{L/2} [1 - p(\xi)] \rho(x) dx, \quad (\text{C5})$$

If we define the surface charge of the electrode as

$$\sigma^\alpha \equiv \int_{-L/2}^{L/2} p(\xi) \rho dx \quad (\text{C23})$$

and the surface charge of the electrolyte as

$$\sigma^\beta \equiv \int_{-L/2}^{L/2} [1 - p(\xi)] \rho dx, \quad (\text{C6})$$

Eq. (C5) recovers the classical electrochemical adsorption formula of Eq. (19). Note that because the total charge is zero,  $\sigma^\alpha = -\sigma^\beta$ .

#### APPENDIX D: GOUY-CHAPMAN-STERN

It is useful to perform a detailed comparison to the standard Gouy-Chapman model of the double layer. This model only treats variations in the electrolyte and the electrode-electrolyte interface is considered to be sharp. The inputs to the model are the difference between the voltage of the electrolyte at the metal  $\phi_0$  and the voltage far from the interface  $\phi_\infty$ , the dielectric constant, and the cation concentration of the electrolyte far from the interface. The Stern modification to the Gouy-Chapman model requires an additional parameter  $x_2$ , the location

of the plane of closest approach to the electrode of ions with a finite radius. The model assumes a Boltzmann distribution in the electrolyte and requires that Poisson's equation be satisfied, giving the voltage as a function of distance from the metal into the electrolyte,

$$\frac{\tanh [z_M \mathcal{F}(\phi - \phi_\infty) / 4RT]}{\tanh [z_M \mathcal{F}(\phi_2 - \phi_\infty) / 4RT]} = \exp [-(x - x_2) / \delta_\phi^{\text{GC}}]. \quad 0 < x_2 < x < \infty \quad (\text{D1})$$

$\phi$  is linear for  $0 < x < x_2$  and  $\phi_2$  is the potential at  $x_2$  obtained by requiring continuity of  $\phi$  and of  $\nabla\phi$  at  $x_2$ . The Debye length of the system is

$$\delta_\phi^{\text{GC}} = \left( \frac{\epsilon RT}{2C_M^\infty z_M^2 \mathcal{F}^2} \right)^{1/2}. \quad (\text{D2})$$

From Gauss' law

$$\sigma^\alpha = -\sigma^\beta = -\epsilon \left( \frac{d\phi}{dx} \right)_{x=x_2} \quad (\text{D3})$$

and Eq. (D1), the surface charge in the metal as a function of  $\phi_2$  is

$$\sigma^\alpha = (8\epsilon C_M^\infty RT)^{1/2} \sinh \frac{z_M \mathcal{F}(\phi_2 - \phi_\infty)}{2RT} \quad (\text{D4})$$

and from Eq. (20), the differential capacitance as a function of  $\phi_2$  is

$$\frac{1}{C_d} = \left[ \left( \frac{2z_M^2 \mathcal{F}^2 \epsilon C_M^\infty}{RT} \right)^{1/2} \cosh \frac{z_M \mathcal{F}(\phi_2 - \phi_\infty)}{2RT} \right]^{-1} + \frac{x_2}{\epsilon} \quad (\text{D5})$$